V European Conference on Computational Fluid Dynamics
ECCOMAS CFD 2010
J. C. F. Pereira and A. Sequeira (Eds)
Lisbon, Portugal,14-17 June 2010

PREDICTING COMPLEX TURBULENT FLAMES USING LARGE EDDY SIMULATION AND FLAMELET-BASED TABULATED CHEMISTRY

Clemens Olbricht*, Frederik Hahn*, Anja Ketelheun* and Johannes Janicka*

*Institute of Energy and Power Plant Technology,
Darmstadt University of Technology,
Petersenstrasse 30, 64287 Darmstadt, Germany
e-mail: ketelheun@ekt.tu-darmstadt.de

Key words: Large eddy simulation, Tabulated chemistry, Turbulent combustion, Sydney flame series, Generic gas turbine combustors

Abstract. *Large Eddy Simulation (LES) and flamelet-based combustion models were applied to four bluff body stabilized nonpremixed and partially premixed flames selected from the Sydney flame series and two generic gas turbine combustors. Unswirled and swirled cases of the Sydney flames were investigated, which exhibited different flow features, such as recirculation, jet precessing and vortex breakdown. Due to various fuel compositions, flow rates and swirl numbers, the combustion characteristics of the flames varied greatly. For all flame calculations good agreement of the main flow features with the measured data was achieved. For purely nonpremixed flames burning attached to the bluff body's outer edge, flamelet modeling including strain rate effects provided good results for the flow field and for most scalars. The prediction of a partially premixed swirl flame could only be achieved by applying a flamelet-based progress variable approach.*
The gas turbine combustors feature different recirculation mechanisms to stabilize the flame. First, a non-swirled combustor with recirculation due to a high-speed air flow was investigated. The second configuration exhibits a complex swirl nozzle inducing the recirculation. In both cases the LES predictions provide good agreement with the experimental data. It turned out that a reasonable spatial resolution in the vicinity of the flame together with TVD-based discretization and standard presumed probability density modeling is sufficient to capture accurately the complex flame lift mechanisms for reactive flows stabilized by hot gas recirculation.

1 INTRODUCTION

Understanding mixing and combustion dynamics has become increasingly important, particularly for achieving high efficiency and low emissions in modern gas turbines and other technical combustion devices. Whenever turbulent nonpremixed combustion takes place, the physical processes typically cover a wide range of time and length scales. Main geometrical features of technical flow systems, like swirl generators or bluff-bodies, induce recirculation zones to stabilize the flame and intensify the mixing of fuel and oxidizer. This frequently goes along with large-scale, coherent fluid motion. To capture those instationary motions the large eddy simulation (LES) technique is commonly used and becomes more and more important in industrial applications[1]. It has great potential in predicting these flow properties, due to a direct simulation of large fluid structures while only nonresolved small scales are modeled. Information about the small scales is required to account for subgrid scale (SGS) mixing. Assumed shape PDF approaches belong to the well-established subgrid scale models for nonpremixed combustion. Together with flamelet-based combustion models such PDF approaches build a popular concept used to account for the variable fluid properties as a result of subgrid scale mixing and chemical reaction. The attractiveness of this concept relies on the utilization of complex chemical mechanisms to build databases, which are parameterized by the mixture fraction for a set of strain rates or a reaction progress variable. This approach allows the separation of hydrodynamic calculations from the solution of stiff chemical systems. The standard approach to model chemical reactions in the LES context are steady (nonpremixed) flamelet models applying a mixture fraction variable only. However, they are conceptually unsuitable to describe flames deviating from chemical equilibrium, showing local extinction, partial premixing or lifted flames. The flames always burn attached to the nozzle due to the "mixed-is-burnt" assumption. A promising concept for simulating such systems relies in progress variable approaches (PVA) where an additional scalar controls the progress of the reaction. Here, the chemistry is parameterized as a function of the mixture fraction and a progress variable[2].

In this study, LES and different flamelet-based combustion models were applied to four bluff body stabilized nonpremixed and partially premixed flames selected from the Sydney flame series[3–8]. Both unswirled and swirled cases were investigated, which exhibit different flow features, such as recirculation, jet precessing and vortex breakdown. Due to various fuel compositions, flow rates and swirl numbers, the combustion characteristics of the flames varied greatly. Different combustion models, flamelet with one or multiple strain rates and a progress variable approach, were applied to these flames. For all flame calculations good agreement of the main flow features with the measured data was achieved. For purely nonpremixed flames burning attached to the bluff-bodys outer edge, flamelet modeling including strain rate effects provided good results for the flow field and for most scalars. The prediction of a partially premixed swirl flame could only be achieved by applying a flamelet-based progress variable approach. Furthermore, the

progress variable approach was applied to two confined model gas turbine combustors to assess its prediction capabilities for lean partially premixed lifted flames. These configurations feature different recirculation mechanisms to stabilize the flame. First, a non-swirled combustor with recirculation due to a high-speed air flow was investigated[9;10]. The second configuration exhibits a complex swirl nozzle inducing the recirculation and coherent vortical structures[11;12]. In both cases the LES predictions provide good agreement with the experimental data. It turned out that a reasonable spatial resolution in the vicinity of the flame together with TVD-based discretization and standard presumed probability density modeling is sufficient to capture accurately the complex flame lift mechanisms for reactive flows stabilized by hot gas recirculation.
The subsequent section 2 deals with the modeling of flow, chemistry and their interaction via presumed PDF and describes the numerical procedure as it is implemented in the FASTEST-ECL code. In section 3 the experimental and numerical setup of the Sydney bluff-body and swirl burner, as well as the generic gas turbine combustors are given. Section 4 presents and discusses the computational results and compares them to experimental data. Some conclusions are drawn in section 5.

2 MODELING

2.1 Governing Equations

Many technical configurations are characterized by low Mach numbers, meaning that the occurring fluid velocities are low compared to the speed of sound. For combustion systems the flow fields can be described by a given set of transport equations in combination with information on the thermo-chemical state. The thermo-chemistry can be provided by tabulated chemical databases relating density and viscosity to a set of scalars. This relation is equivalent to the equation of state (EOS) in compressible flows.
Even though in implicit LES no explicit filtering is applied to the conservation equations or the results, the technique itself is naturally only able to solve for the grid resolved turbulent scales. To account for this implicit filter the equations have to be filtered in advance. In the case of variable density flows typically a density weighted filtering $\bar{\rho}\widetilde{\varphi} = \overline{\rho\varphi}$ (Favre filtering) is performed. Applying this formalism to the conservation equations of continuity and momentum with the density ρ, the kinematic viscosity ν, the velocity vector u_i and the pressure p, these read as:

$$\frac{\partial \bar{\rho}}{\partial t} + \frac{\partial}{\partial x_j}(\bar{\rho}\,\widetilde{u}_j) = 0 \tag{1}$$

$$\frac{\partial}{\partial t}(\bar{\rho}\,\widetilde{u}_i) + \frac{\partial}{\partial x_j}(\bar{\rho}\,\widetilde{u}_i\,\widetilde{u}_j) = \frac{\partial}{\partial x_j}\left(\bar{\rho}\,\widetilde{\nu}\left(\frac{\partial \widetilde{u}_i}{\partial x_j} + \frac{\partial \widetilde{u}_j}{\partial x_i} - \frac{2}{3}\frac{\partial \widetilde{u}_k}{\partial x_k}\,\delta_{ij}\right) + \bar{\rho}\,\tau_{ij}^{sgs}\right) - \frac{\partial \bar{p}}{\partial x_i} \tag{2}$$

A transport equation for any scalar ϕ with D_ϕ denoting the transport coefficient and S_ϕ any source term, e.g. chemical source term, can be written as:

$$\frac{\partial}{\partial t}(\bar{\rho}\,\widetilde{\phi}) + \frac{\partial}{\partial x_j}(\bar{\rho}\,\widetilde{u}_j\,\widetilde{\phi}) = \frac{\partial}{\partial x_j}\left(\bar{\rho}\left(\widetilde{D}_\phi\,\frac{\partial\widetilde{\phi}}{\partial x_j} + J^{sgs}_{\phi,j}\right)\right) + \widetilde{S}_\phi \tag{3}$$

Due to the filtering operation additional terms τ^{sgs}_{ij}, $J^{sgs}_{\phi,j}$ arise in equations (2) and (3), accounting for the momentum and scalar flux at sub filter level. These contributions have to be modeled. The subgrid scale stress tensor τ^{sgs}_{ij} in equation (2) is closed by a Smagorinsky model[13]. The deviatoric part is modeled based on an eddy-viscosity assumption, while the isotropic part is included into the pressure term, resulting in the pressure parameter $\overline{P}$.

$$\tau^{sgs}_{ij} - \frac{1}{3}\tau^{sgs}_{kk}\delta_{ij} \approx 2\,\nu_t\,(\widetilde{S}_{ij} - \frac{1}{3}\widetilde{S}_{kk}\delta_{ij}) \quad \text{with} \quad \nu_t = \left(C_S\bar{\Delta}\right)^2\left|\widetilde{S}_{ij}\right| \tag{4}$$

$$\widetilde{S}_{ij} = \frac{1}{2}\left(\frac{\partial\widetilde{u}_i}{\partial x_j} + \frac{\partial\widetilde{u}_j}{\partial x_i}\right) \tag{5}$$

$$\overline{P} = \overline{p} - \frac{\overline{\rho}}{3}\tau^{sgs}_{kk} \tag{6}$$

The model coefficient C_S in eq. (4) for the turbulent viscosity ν_t is obtained by the dynamic procedure proposed by Germano et al.[14] and using the least-squares approach following Lilly[15]. No special wall treatment is included into the sub-grid scale model. The approach relies on the dynamic procedure to reproduce the correct asymptotic behavior of the turbulent flow near the wall[16]. In equation (3) the contribution of the subgrid scalar fluxes can be modeled consistently with the modeling of the subgrid scale stresses with a gradient flux approach,

$$J^{sgs}_{\phi,j} \approx \frac{\nu_t}{\sigma_t}\frac{\partial\widetilde{\phi}}{\partial x_j}. \tag{7}$$

Here, a subgrid scale Schmidt number σ_t relates the turbulent diffusion coefficient to the turbulent viscosity ν_t.

2.2 Combustion Modeling

The mixture fraction concept was used to account for two species mixing as present in nonpremixed or partially premixed combustion systems. A transport equation for the mixture fraction can be derived from equation (3), assuming equal diffusivities $D_\alpha = D$ for all species.

$$\frac{\partial}{\partial t}(\bar{\rho}\,\widetilde{f}) + \frac{\partial}{\partial x_j}(\bar{\rho}\,\widetilde{u}_j\,\widetilde{f}) = \frac{\partial}{\partial x_j}\left(\bar{\rho}\left(\widetilde{D}\,\frac{\partial\widetilde{f}}{\partial x_j} + J^{sgs}_{f,j}\right)\right) \tag{8}$$

Due to the definition of the mixture fraction based on element mass fractions equation (8) contains no source term. Hence, f can be considered to be a conserved scalar.

The flamelet concept is based on the idea that turbulent flames are composed of tiny laminar flames, the "flamelets". Peters[17] derived a steady flamelet equation by transforming equation (3) into mixture fraction space. Steady flamelets can be parameterized by the mixture fraction f and the scalar dissipation rate χ. Thus, the steady flamelet database yields

$$\Phi_{SF} = \Phi(f, \chi). \tag{9}$$

Assuming infinitely fast chemistry, unity Lewis numbers ($Le = D_\alpha \rho c_p / \lambda = 1$) and no heat losses, it appears that the species composition, the temperature and the enthalpy can be described by the mixing process only. Due to the fact that the scalar dissipation rate can be interpreted as an inverse mixing time it is suitable to account for non-equilibrium concentrations. The filtered scalar dissipation rate can be modeled following an algebraic approach proposed by Girimaji and Zhou[18]:

$$\widetilde{\chi} = 2\left(D + \frac{\nu_t}{\sigma_t}\right)\frac{\partial \widetilde{f}}{\partial x_j}\frac{\partial \widetilde{f}}{\partial x_j} \tag{10}$$

One of the main disadvantages of the standard steady flamelet approach is that it does not cover the whole range from pure mixing (extinction) to chemical equilibrium. Solely burning solutions are incorporated in this concept and lead to a "mixed-is-burnt"-like behavior. Thus, it is not suitable when accounting for complex burning situations like flame lift, local extinction, re-ignition, etc.
A further developed flamelet-based reduction technique takes advantage of a scalar variable controlling the chemical progress. Van Oijen and de Goey[19] proposed a mixture fraction/progress variable approach (PVA) which is based on the solution of steady premixed flamelets building a premixed flamelet-generated manifold (FGM). Recent studies[19;20] revealed that premixed FGMs are also applicable to premixed and nonpremixed combustion systems. In van Oijen and de Goey's approach the progress variable is typically a linear combination of weighted reaction product species α,

$$\mathcal{Y} = \sum_\alpha \frac{Y_\alpha}{M_\alpha}. \tag{11}$$

with the species mass fractions Y_α and the molar mass M_α. The source term for the progress variable is evaluated accordingly. To build well-defined databases this progress variable has to be selected monotonically increasing with the reaction progress for each flamelet. The chemical database Φ is then parameterized by the mixture fraction f and the progress variable $\mathcal{Y}$, leading to

$$\Phi_{FGM} = \Phi(f, \mathcal{Y}). \tag{12}$$

Outside the flammability range all thermo-chemical variables have to be extrapolated to the limits of possible mixtures ($f = 0, \ldots, 1$).

2.3 PDF Modeling

Knowledge of subgrid distributions of scalars which constitute the chemical database is required when accounting for unresolved scales. Due to a generally nonlinear relation of Φ to these scalars, an integration of the subgrid probability density function (PDF) is necessary to achieve filtered thermo-chemical properties $\widetilde{\Phi}$. In the case of steady flamelet modeling the PDF is defined by $P(f,\chi)$. Assuming statistical independence of f and χ yields $P(f,\chi) = P(f) \cdot P(\chi)$. Hence, the distributions can be modeled separately. A commonly used approach is to apply a presumed β-PDF to the distribution of the mixture fraction and a Dirac δ-function to the distribution of the scalar dissipation rate[2]. With these assumptions and the subgrid variance $\widetilde{f''^2}$ the filtered thermo-chemical properties read as

$$\widetilde{\Phi(f,\chi)} = \iint \phi(f,\chi)\beta(f;\widetilde{f},\widetilde{f''^2})\delta(\chi;\widetilde{\chi})\,\mathrm{d}f\mathrm{d}\chi = \widetilde{\Phi}(\widetilde{f},\widetilde{f''^2},\widetilde{\chi}). \tag{13}$$

The subgrid variance is modeled according to Branley and Jones[21]. This model employs a new model constant C_ν, which is suggested by Branley and Jones to be in the range of 0.1 to 0.2.

$$\widetilde{f''^2} = C_\nu \Delta \frac{\partial \widetilde{f}}{\partial x_j}\frac{\partial \widetilde{f}}{\partial x_j} \tag{14}$$

In the case of the PVA, a subgrid PDF modeling approach according to Landenfeld et al.[22] is used. In nonpremixed flames where complex flame effects like local extinction or flame lift do not appear, a strong correlation between f and $\mathcal{Y}$ can be expected. A PDF modeling according to equation (13) with a separation of the PDF is then unsuitable. The Landenfeld et al. method is based on minimizing the statistical dependency of the tabulated variables. Therefore, the progress variable is normalized by its maximum value $\mathcal{Y}_{max}$ resulting in a reaction progress variable C ranging from zero to one.

$$C = \frac{\mathcal{Y}}{\mathcal{Y}_{max}} \tag{15}$$

The new manifold is then built as $\Phi_{FGM} = \Phi(f,C)$. With this technique the correlation between the tabulated variables f and C can be reduced strongly. Applying a Dirac δ-function to the distribution of C and a presumed β-PDF to the distribution of the mixture fraction the filtered thermo-chemical properties read as

$$\widetilde{\Phi(f,C)} = \iint \phi(f,C)\beta(f;\widetilde{f},\widetilde{f''^2})\delta(C;\widetilde{C})\,\mathrm{d}f\mathrm{d}C = \widetilde{\Phi}(\widetilde{f},\widetilde{f''^2},\widetilde{C}). \tag{16}$$

The filtered reaction progress variable is evaluated using the same assumed shape PDF as in equation (16). According to Landenfeld et al.[22] cross-correlations of $\mathcal{Y}$ and $\mathcal{Y}_{max}^{-1}$ can be neglected.

$$\widetilde{C} \approx \widetilde{\mathcal{Y}} \cdot \widetilde{\left(\frac{1}{\mathcal{Y}_{max}}\right)} \quad \text{and} \quad \widetilde{\left(\frac{1}{\mathcal{Y}_{max}}\right)} = \int \left(\frac{1}{\mathcal{Y}_{max}}\right)\beta(f;\widetilde{f},\widetilde{f''^2})\,\mathrm{d}f \tag{17}$$

2.4 Numerical Procedure

The governing equations were implemented in the three dimensional low-Mach number LES code FASTEST-ECL. The code uses geometry flexible, block-structured, boundary fitted grids, enabling it to represent complex geometries. A co-located grid with a cell-centered variable arrangement is used. The flow solver offers fully second order accuracy. Discretization is based on the finite volume method. For spatial discretization, specialized central differencing schemes, which preserve second order for arbitrary grid cells are used[23]. To assure boundedness of the mixture fraction, the convective term in the scalar transport has been discretized using non-oscillatory, bounded TVD schemes[24]. Multiple stage Runge-Kutta schemes with second order accuracy are used for the time stepping. A fractional step formulation is applied and at each stage a momentum correction is carried out in order to satisfy continuity. Therefore a Poisson equation is derived from equation (1) and solved iteratively with multi-grid and SOR relaxation. For the turbulent Schmidt number σ_t=0.7 and for the variance model constant C_ν=0.15 were chosen. The steady flamelet databases were built using the one dimensional flow solver CHEM1D[25]. For this purpose, steady, laminar opposed jet flames were solved for strain rates, starting from $a = 10\,\mathrm{s}^{-1}$ to the last burning strain rate $a = 1660\,\mathrm{s}^{-1}$. In the case of FGM modeling steady laminar premixed flames were calculated within the flammability limits. Outside these limits an extrapolation method by Ketelheun[26] which is based on preserving physical solutions in too lean or too rich regions was used. For all FGM calculations CO_2 has been used as progress variable. For the flamelet computations the GRI 3.0 chemical mechanism[27] with Le_α=1 was applied. The resulting scalar values were mapped on mixture fraction and dissipation rate or progress variable coordinates, respectively.

3 EXPERIMENTAL AND NUMERICAL SETUP

3.1 Sydney Bluff-Body Burner

The Sydney bluff-body swirl configuration, with all dimensions and the coordinate system, is shown in Figure 1. For the unswirled cases no annulus is present. The rotationally symmetric bluff-body nozzle is housed in a square duct of 130 mm to 305 mm width, depending on the flow case. Gas is fed through a centered pipe at a bulk jet velocity of u_j at ambient conditions with a Reynolds number of Re_j. In the case of swirl configurations, swirled air is injected through an annular gap (primary air flow: axial component u_s, rotational component w_s). The geometric swirl number S_g is evaluated with the mean bulk velocities (w_s/u_s) within the annular gap. The secondary air stream (ambient conditions, co-flow) between the duct and the burner nozzle is fixed at u_c. The measurements were conducted by Dally et al.[3;4], Kalt et al.[5], Al-Abdeli and Masri[6;7] and Masri et al.[8] The flow parameters of the four investigated flames are given in Table 1. All simulations were carried out on elliptically smoothed hexahedral grids. For the unswirled bluff-body configuration two grids with 1.1 and $2.2{\cdot}10^6$ grid points (GP) and for the swirled bluff-body case three grids (1.1, 2.2 and $2.7{\cdot}10^6$ GP) were created. The special three-dimensional

Flame	Fuel	f_{st} $(-)$	u_c (ms^{-1})	u_s (ms^{-1})	u_j (ms^{-1})	Re_s $(-)$	Re_j $(-)$	S_g $(-)$	L_f (m)
HM1E	CH_4/H_2 (1:1)	0.050	35.0	-	108.0	-	15800	-	1.00
HM3E	CH_4/H_2 (1:1)	0.050	35.0	-	195.0	-	28500	-	1.00
SM1	CH_4	0.055	20.0	38.2	32.7	75900	7200	0.50	0.12
SMA2	CH_4/Air (1:2)	0.250	20.0	16.3	66.3	32400	15400	1.59	0.23

Table 1: Flame and flow conditions of the investigated cases of the Sydney flame series.

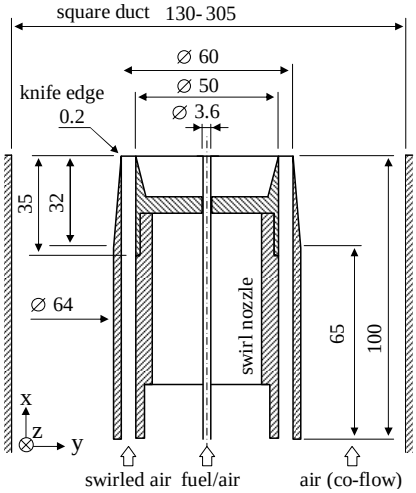

Figure 1: Sketch of the Sydney bluff-body swirl burner (dimensions mm).

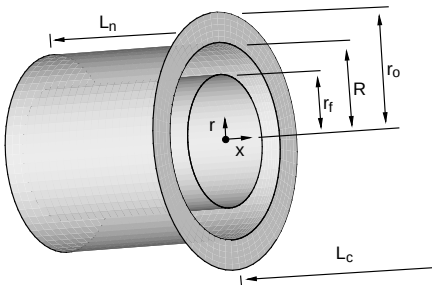

L_N	$95\,mm$
L_C	$1\,m$
r_f	$31.66\,mm$
R	$46.85\,mm$
r_o	$61.15\,mm$

Figure 2: Nozzle dimensions of the Owen et al. combustor.

O-grid arrangements guarantee a very fine resolution within the nozzle, around the bluff-body and the near nozzle region. The computational domain covers the square duct in the lateral direction. In the axial direction, the domain reaches from one bluff-body length D_{bb} upstream to $5.2D_{bb}$ downstream of the jet exit plane in the unswirled case and $10D_{bb}$ in the swirled case. The fuel nozzle is included with a length of approximately 13.8 jet diameters.
At the inlets bulk flow velocities were prescribed for the jet. In the case of the unswirled bluff-body flows artificial turbulence was superimposed for the coflow using the method of Klein et al.[28]. For the swirled cases no artificial turbulence was used. At the exit plane a convective outlet boundary condition was prescribed.

3.2 Generic Gas Turbine Combustors

3.2.1 Owen et al. Combustor

The nozzle of the axisymmetric combustor experimentally investigated by Owen et al.[9] is shown in Figure 2, including its dimensions. The combustion chamber had a length of

Fuel	u_f (ms^{-1})	Re_f $(-)$	T_f (K)	u_o (ms^{-1})	Re_o $(-)$	T_o (K)	p (bar)	ϕ $(-)$	$\frac{(\rho u)_f}{(\rho u)_o}$ $(-)$
CH_4	0.9287	10000	300	20.63	95000	750	3.8	0.9	0.063

Table 2: Operating conditions of the Owen et al. combustor. Inlet velocities u, Reynolds numbers Re, temperatures T for fuel (index f) and oxidizer (index o), combustor pressure p, equivalence ratio ϕ and momentum ratio of fuel and oxidizer.

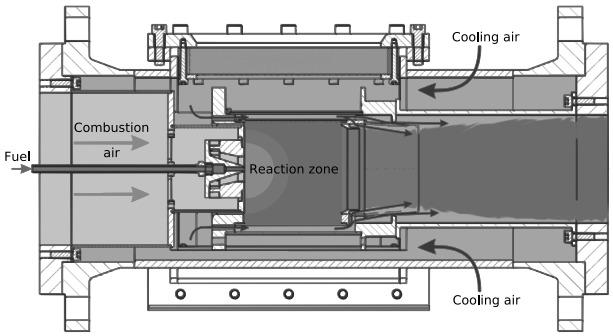

Figure 3: Setup of the Janus et al. combustor.

$1000\,mm$ in the experiment, for the computation it was only included for $375\,mm$. The nozzle diameter R is used to normalize length scales in the remainder of this paper. The operating conditions are listed in Table 2. Preheated air is fed to the combustion chamber through a coaxial annulus. The fuel in the central nozzle, being natural gas ($\approx$96 % CH_4), is not preheated. The separation between fuel and air was modeled as infinitely thin wall in the simulation. Porous discs were used to homogenize the flow inside the nozzles. The combustor walls are water cooled and feature nearly uniform wall temperatures of $500\,K$. Due to the high difference of axial momentum of fuel and oxidizer the fuel outlet figures as bluff-body inducing a central recirculation zone. Owen et al. observed large-scale fluctuations or coherent structures resulting from low frequency movements of the recirculating gas into the fuel nozzle. Gas bubbles enter the fuel nozzle on one side and partially block it. In the other parts of the nozzle increased eddy breakup is observed, leading to stronger mixing in the shear layers and thus lifting of the flame.
As for the Sydney flames, an elliptically smoothed grid with three-dimensional O-grid arrangements was used. The grid consists of $5.1{\cdot}10^6$ grid cells. The nozzle was included for approx. $2R$ in the computational domain, the combustor was included for $8R$, approx. one third of its total length. At the inlet, the bulk flow velocities for fuel and air were prescribed. Artificial turbulent fluctuations obtained by the method of Klein et al.[28] were superposed.

Fuel	$\dot{m}_f$ (kgs^{-1})	$Re_f = Re_o$ $(-)$	T_f (K)	$\dot{m}_o$ (kgs^{-1})	$T_o = T_c$ (K)	$\dot{m}_c$ (kgs^{-1})	p (bar)	ϕ $(-)$	S $(-)$
CH_4	0.00137	26200	368	0.03	623	0.09	2	0.8	1.2

Table 3: Operating conditions of the Janus et al. combustor. Inlet mass flows $\dot{m}$, Reynolds numbers Re and temperatures T for fuel (index f), oxidizer (index o) and cooling air (index c), combustor pressure p, equivalence ratio ϕ and swirl number S.

3.2.2 Janus et al. Combustor

This configuration was extensively experimentally investigated by Janus et al.[11;12]. The setup is shown in Figure 3. Fuel and air are preheated and fed separately into the combustion chamber. From the experiment a lifted flame was reported as well as a coherent structure, forming a helical vortex. Geometrical complexity arises not only from the included swirler, but also from the asymmetry of the combustor itself due to the optical accessibility. The operating conditions are summarized in Table 3. As the temperature of the cooling air was not exactly known from the experiment, it was assumed to be equal to the temperature of the oxidizing air.
The employed grid used a three-dimensional O-grid structure, as for the other configurations, was elliptically smoothed and contained approx. $2{\cdot}10^6$ grid cells. Bulk flow velocities were prescribed at the inlet boundary conditions without adding artificial turbulence. The direction of the velocity vectors at the swirler inlet was defined parallel to the channels. The cooling air velocity is defined normal to the inlet surface.

4 RESULTS

4.1 Sydney Bluff-Body Burner

The "simplest" flame of this series is the methane-hydrogen flame HM1E which is stabilized by two counter-rotating vortices forming a recirculation zone behind the bluff-body. The inner vortex feeds this zone with fresh fuel, while the outer vortex entrains hot gases. Between the vortices fuel is preheated. The flame is 50% of the flowrate of extinction. The outer surface of the bluff-body generates vortex-shedding, which influences the reaction zone and enhances velocity fluctuations. Further downstream the jet penetrates through the recirculation zone. There, intense mixing takes place, and as a consequence strong turbulence-chemistry interactions are present. In this region a secondary reaction zone is established and HM1E behaves like a normal jet flame. Due to the interaction of recirculation zone and jet, the flame length as well as the temperature fluctuates strongly. The flame HM3E differs from HM1E in having a higher jet Reynolds number and hence exhibiting much stronger turbulence-chemistry effects. The jet-flame-like behavior is established much earlier in this case, leading to significant local extinction events in the region downstream of the bluff-body wake. The flame is 10% from extinction. Because of the higher jet velocity the bluff-body recirculation is more compact providing the mixing of fuel and hot gases. The entrainment of air is increased so that higher temperatures

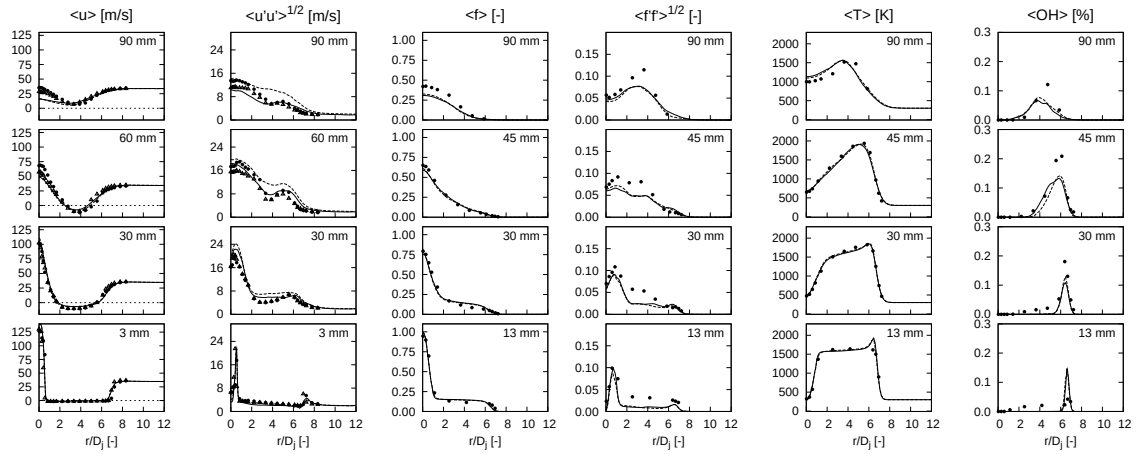

Figure 4: Flame HM1E. Time averaged results of axial velocity and mixture fraction (mean values and fluctuations), temperature and OH (mean values). •, △ Experiment, – – – LES-OF, — LES-MF.

within the wake can be obtained. Also the constriction is much stronger than in HM1E. The swirl flames exhibit further fluid dynamic features which superimpose on the mechanisms present in the unswirled cases. Intensified or additional recirculation zones lead to more compact, shorter flames. Due to a vortex breakdown mechanism in flame SM1 a secondary reaction zone is established at the axis. The interaction of the vortex breakdown bubble (VBB) with the fuel jet leads to strong jet precession. Because of a relatively low stoichiometry the swirl flame burns attached to the bluff-body's outer edge. The bluff-body recirculation is not as developed in flame SM1 as in the unswirled flames.
Because of a partially premixed jet the burning behavior of SMA2 differs strongly from that of the other flames. The stoichiometry is much higher, hence the flame burns right above the bluff-body between the inner and the outer edge. In contrast to SM1, vortex breakdown is not present. Because of a highly swirled primary air flow with a low axial momentum, in conjunction with a high jet momentum, a very strong recirculation zone above the bluff-body is formed. The recirculation zones due to hydrodynamics and geometry overlap. The formation of a vortex breakdown mechanism is suppressed by a high momentum flux ratio of the axial jet and the primary air.

4.1.1 Bluff-Body Flame HM1E

In Figure 4 the calculated time-averaged axial velocity and the mixture fraction and their fluctuations, as well as the temperature and the hydroxyl (OH) concentration are compared to experimental data. For the axial velocity component an overall good agreement can be obtained. The jet penetration depth, the spreading and the positions of the two shear layers are predicted quite well. The jets maximum velocity decays a little too fast. The bluff-body wake is predicted correctly by all computations. For the velocity distinct differences between the computations were not observable. For the time-averaged

axial and radial velocity fluctuations an overall good agreement can be obtained, with little difference between the two calculations. The position and level of the fluctuations within the inner shear-layer is predicted correctly.
Scalar data for HM1E is not available, only for the similar flame HM1. The flames HM1 and HM1E are both 50% of blow-off and it was found that the flow fields differ only marginally and computations yield almost identical scalar fields[29]. For the mixture fraction an overall good agreement has been obtained as well. The penetration length is predicted with acceptable accuracy and the plateau type structure close to the bluff-body with a nearly constant mixture fraction value is captured well by all LES. Further downstream the mixture fraction is somewhat overestimated, later the decay rate is too high. Generally the fluctuations of the mixture fraction are underestimated, whereas profiles, peak values and positions are satisfactory. For the fluctuations the two LES provide small differences, but there is no clear trend.
According to Kempf et al.[29] and Raman et al.[30] a temperature peak is predicted at the position $x = 13\,mm$, $r/D_j = 6.9$ by all LES. A very good agreement for the mean temperature can be obtained. Some small differences in the calculations are identifiable for the temperature fluctuations, however without a clear trend. The mean values of the species concentrations mostly show good agreement. There is little difference between the calculations apart from some small improvements within the OH prediction using LES-MF. Even though OH is somewhat underpredicted near the bluff-body, it has been observed that most species are predicted very well within the recirculation zone. Here the residence times are relatively high. Due to this fact, finite-chemistry effects are minimized and the species are well described using steady flamelets. It is remarkable that LES-MF could not lower the OH concentration near the bluff-body edge. The same is observed by Kempf et al.[29] and Raman et al.[31]. Navarro-Martinez and Kronenburg[32] argue that conditional scalar dissipation values around stoichiometric are quite small (around $1\,s^{-1}$). Consequently the OH concentration is only slightly affected by the strain rate.

4.1.2 Bluff-Body Flame HM3E

In contrast to HM1E, consideration of strain rate effects influences the numerical results for HM3E strongly. Due to high dissipation rates above $x = 50\,mm$ strong local extinction is present which cannot be captured by the OF approach. A shift to the LES-multiple flamelet (MF) approach provided improved results. Figure 5 shows the time-averaged velocity and mixture fraction profiles and their fluctuations. Both computations (OF, MF) are compared to the experimental data. For the axial velocity component both provide good results. The strength and location of the recirculation zone and the gradients are predicted with good accuracy. For these features LES-MF offers slightly better results. The fluctuations at the first measurement plane are in good agreement with the experimental data. It seems that the turbulence level of the inner shear-layer is overpredicted at $x = 4\,mm$ and continued further downstream. Above $x = 4\,mm$ both modeling

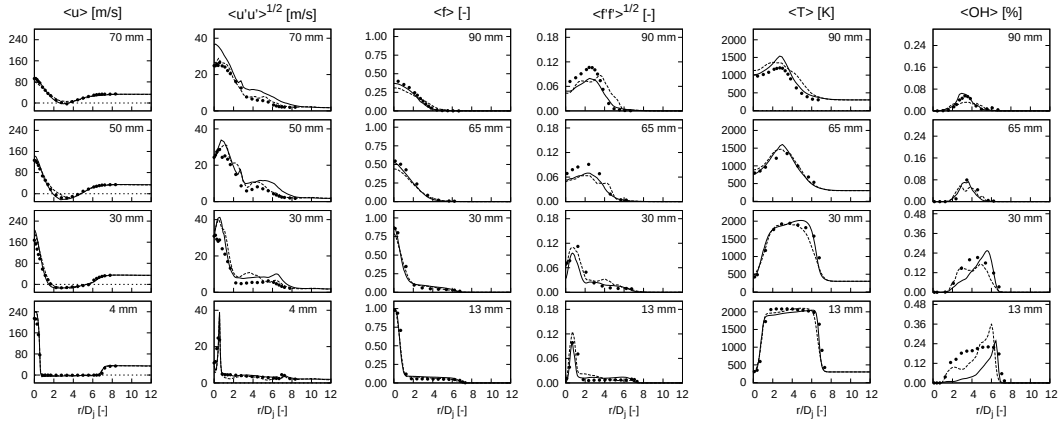

Figure 5: Flame HM3E. Time averaged results of axial velocity and mixture fraction (mean values and fluctuations), temperature and OH (mean values). • Experiment, – – – LES-OF, — LES-MF.

approaches have difficulties in predicting the correct level of the velocity fluctuations, but still the shape, peak positions and the order of magnitude agree with the measurements. The LES-MF approach provides an almost correct penetration behavior of the mixture fraction. Surprisingly the mixture fraction fluctuations are mostly underestimated by both approaches, in contrast to what has been observed for the velocity field. Figure 5 additionally shows the temperature and the species concentration of OH. The scalar quantities like mixture fraction and temperature benefit strongly from the incorporation of multiple flamelets. The temperature is predicted with good accuracy showing matching data along the axis. In contrast to the OF modeling the LES-MF approach offers improved predictions for the temperature gradients, although the temperature peaks above $x = 65\,mm$ are somewhat higher. The high temperature plateau directly above the bluff-body is captured well, with slight deviations towards the axis. The temperature fluctuations obtained with LES-MF are predicted with good accuracy. In contrast to the experiments both models estimate the flame burning mainly towards the outer edge right above the bluff-body. In consideration of the complexity of this quantity the hydroxyl radical is predicted excellently downstream of the bluff-body from $x = 30\,mm$. Here the LES-MF approach provides improved results.

4.1.3 Swirl Flame SM1

The methane-air swirl flame SM1 exhibits a complex, highly instationary flow characteristic. Thus intense turbulence chemistry interactions are expected for that flame. Three computations of SM1, with one and with multiple flamelets including strain effects, as well as with FGM modeling, were carried out. In the case of FGM combustion modeling a PDF assumption different from equation (16) has been used. Here, statistical independence of the mixture fraction and the physical progress variable has been

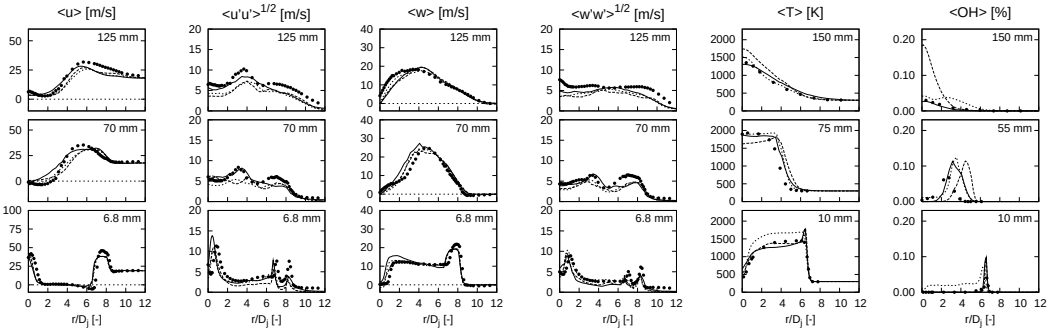

Figure 6: Flame SM1. Time averaged results of axial and rotational velocity component (mean values and fluctuations), temperature and OH (mean values). • Experiment, – – – LES-OF, — LES-MF, - - - LES-FGM.

assumed[33]. Figure 6 shows the time-averaged velocities and their fluctuation. The overall agreement is quite good. The LES-MF calculation offers a clear improvement in predicting the fluctuations. Shape and peak positions almost match the experimental data. The decay of the jet is predicted well by all simulations. It seems that the experimental data show a bias towards higher radii. Again, the vortex breakdown phenomenon is captured by all calculations. Results of the temperature and OH are shown in Figure 6 as well. As expected, a clear improvement on the calculations with LES-OF was provided by the LES-MF calculation. With the LES-FGM approach a similar spreading behavior to that of the LES-MF was observed. At positions away from the bluff-body and at the centerline this approach provides strongly improved results. Due to the absent diffusion in mixture fraction space within the premixed FGM database the near equilibrium values within the bluff-body recirculation rise too high. For the temperature both dissipation rate based simulations predict a too intense reaction at the outer shear-layer as indicated by the peaks of all quantities at the first measurement plane. A slight deviation of the mixture fraction can lead to significant errors in temperature and scalar predictions. Here, a slight deviation in predicting the mixture fraction gradient towards the recirculation plateau causes a temperature and species peak. Within the LES-FGM calculation this distinct peak does not appear. The LES-OF approach overestimates the strength of the secondary reaction zone which is most evident in the OH concentration at $x = 150\,mm$. Applying LES-MF or LES-FGM reduces the OH concentration drastically towards the measured values.

4.1.4 Swirl Flame SMA2

In previous investigations Olbricht et al.[34] showed that dissipation rate based flamelet approaches fail in predicting this flame. Using such approaches leads to a flame burning within the inner shear-layer where stoichiometry is reached. In fact, the flame propagates from the inner to the outer shear-layer. Right above the burner's base significant OH is

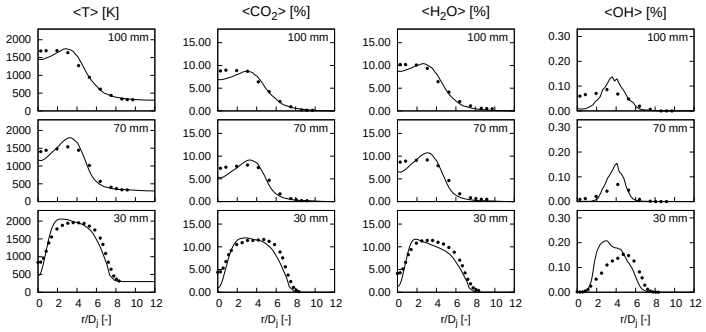

Figure 7: Flame SMA2. Time averaged mean values of temperature, CO_2, H_2O and OH profiles. • Experiment, — LES-FGM.

present, which indicates a widespread reaction zone. This issue, together with the strong bluff-body recirculation, forms a high temperature region. Hence, only results of the more sophisticated LES-FGM approach are shown. For the PDF modeling, the formulation proposed in section 2.3 is adopted. A vortex breakdown mechanism has not been observed by the LES-FGM and the experiments. Figure 7 shows time-averaged temperature, CO_2, H_2O and OH results of the LES-FGM and the experiments. Good agreement with the experimental data is observable. A general problem is in achieving the correct centerline values, as they are mainly underpredicted. Within the recirculation zone the results are of good quality. The temperature level at $x = 30\,mm$ is predicted well whereas the plateau type shape towards the axis further downstream could not be captured correctly. The temperature gradients at the outer shear-layer obtained by the LES-FGM match with the experiments quite nicely. The hydroxyl radical OH is distributed in the whole area above the bluff-body. However, there are deviations from the measured values. The OH production mechanism of this species can be comprehended with the available results. The location of the flame-front as well as its strength is captured reasonably by the proposed LES-FGM approach.

4.2 Generic Gas Turbine Combustors

4.2.1 Owen et al. Combustor

Figure 8 shows a quantitative comparison of the computational results to the experimental data. The radial and axial positions are normalized by the nozzle diameter R. The two left columns show the time averaged mean and fluctuations of the axial velocity. They are normalized with the inflow velocity of the air, u_{Ox}. The position and the strength of the recirculation zone are well captured. The recirculation zone was observed between $x/R = 0.42$ and $x/R = 2.34$. At the third position at $x/R = 1.27$, the very good matching of the gradients can be observed. Noticeable is the good agreement at the last measurement plane at $x/R = 4.67$. Here, the cumulation of the heat release in the flame and the resulting thermal expansion strongly influence the velocity. The velocity fluctua-

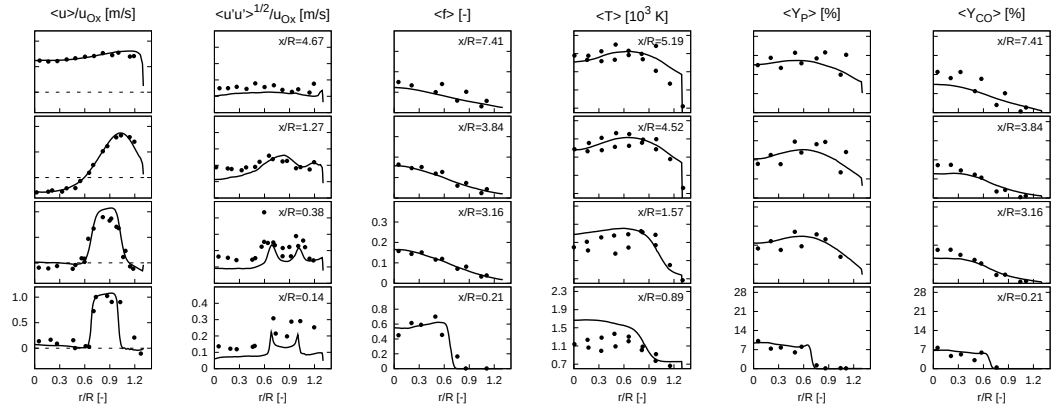

Figure 8: Owen et al. combustor. Time averaged mean values and fluctuations of axial velocity, mean values of mixture fraction, temperature, product mass fraction and CO. • Experiment, — LES-FGM.

tions are too low above the fuel outlet. However, a plateau-shape of the fluctuations even in regions without velocity gradients can be observed. According to Owen et al. this can be ascribed to large scale coherent structures leaving the outlet plane. The third column of Figure 8 shows the mean values of the mixture fraction. The mixing of oxidizer air and hot exhaust gas with the cold fuel because of the recirculation into the fuel nozzle is well represented by the computation. This indicates a good prediction of the heat release. The mean temperature, a reaction product mass fraction ($y_P = y_{H_2O} + y_{CO_2}$) and the carbon monoxide mass fraction are given the three right columns of Figure 8. The too high temperature in the lower measurement positions results from heat loss to the cooled combustor walls and radiation in the experiment which were not included in the simulation. Furthermore, mixing effects conceptually cannot be included in the FGM table. The mean profiles of the product mass fraction and the CO mass fraction match very well with the experimental data, especially behind the recirculation zone. The computational results are of comparable quality to those by Pierce and Moin[10]. Overall, a very good accordance between the simulation and the experiment was observed.

4.2.2 Janus et al. Combustor

Figure 9 shows the time averaged mean values of the axial and tangential velocity components at different measuring positions in the two left columns. The results are normalized with the axial jet velocity u_0 at the inflow. The radial position is normalized by the inner nozzle diameter $D = 6\,mm$. For the mean velocities, a very good agreement with the measured data could be obtained. In comparison to the experiment, a too strong decay of the axial velocity of the fuel jet is observed. The radial velocity component is slightly overpredicted, being the reason for a too strong spreading of the swirl flow. The stagnation point of the fuel jet is found at $x/D = 2.5$. The tangential velocity capture the spreading of the flow well, compared to the experiment. The analysis of the velocity

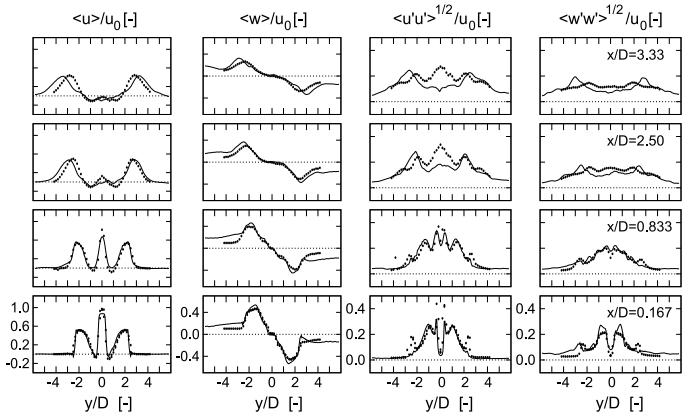

Figure 9: Janus et al. combustor. Time averaged mean values and fluctuations of the axial, and rotational velocity component. • Experiment, — LES-FGM.

fluctuations, given in Figure 9 in the right columns, confirms the impression obtained from the comparison of the mean values. A very good agreement for both the axial and tangential velocity fluctuations is obtained. The amount of the radial fluctuations is overpredicted, compared to the experiment. For both velocity components, the maximum values of the fluctuations are obtained in the shear layers. This indicates that the energy contents of the coherent structure —if it is still present— strongly decays. No significant differences between the first to measuring positions can be observed. At $x/D = 2.50$ and $x/D = 3.33$ the fluctuations observed in the experiments are higher compared to the simulations in the region of the central fuel jet. This effect is not present for the tangential fluctuations. A deviating prediction of the precession of the fuel jet is thus not the reason for the differences. The lower fluctuations of the axial velocity are explained by the lower axial velocity predicted by the simulation. The most challenging part in the prediction of this configuration is the description of position and strength of the central recirculation zone. It has a strong influence on the mean flow field. The remaining uncertainties for the boundary conditions make the correct prediction of the recirculation zone even more difficult.

5 CONCLUSIONS

Progress has been made in predicting Sydney flames and generic gas turbine combustors by applying flamelet-based combustion models. The investigated flames were chosen to differ in stabilization mechanism, flame-front position, flame length, flame lift, distance to blow-off and fuel composition. Based on flamelet reduction techniques, the sophistication of the combustion model was adjusted to fit the requirements of each flame. The hybrid LES-flamelet approaches have been proven to be a reliable tool for the prediction of combustion processes for different flames. A clear trend of utilizing progress variable based flamelet approaches is observable, due their universality. A reduction technique based on premixed generated manifolds was introduced and successfully applied to two swirl

flames and two gas turbine combustors exhibiting different burning behaviors. Standard strain rate based flamelet approaches combined with LES provided very good results for two unswirled and one swirled flame, even for intermediate species and the OH radical. Accurate predictions of complex flows are feasible with the proposed modeling techniques. Also, complex flow features like recirculation, jet precessing or vortex breakdown have been reproduced. As the lifted flames in the combustors are stabilized by recirculation rather than by premixed flame propagation, they are not sensitive towards modeling of the effective burning velocity. As long as the grid is reasonably fine, the TVD scheme and the numerical diffusion lead to a sufficient resolution of the flame front.

ACKNOWLEDGEMENTS

All computations have been performed on the Hessian High Performance Computer (HHLR), which is supported by the High Performance Scientific Computing (HPSC) activity group, a member of the computational engineering center in Darmstadt. The authors gratefully acknowledge the German Research Foundation (DFG) for financial support through the collaborative research center SFB 568.

REFERENCES

[1] J. Janicka and A. Sadiki. Large eddy simulation of turbulent combustion systems. *Proc. Combust. Inst.*, 30:537–547, 2005.

[2] H. Pitsch. Large-Eddy Simulation of Turbulent Combustion. *Annu. Rev. Fluid Mech.*, 38:453–482, 2006.

[3] B. B. Dally, D. F. Fletcher, and A. R. Masri. Flow and mixing fields of turbulent bluff-body jets and flames. *Combust. Theory Modelling*, 2:193–219, 1998.

[4] B. B. Dally, A. R. Masri, R. S. Barlow, and G. J. Fiechtner. Instantaneuos and mean compositional structure of bluff-body stabilized nonpremixed flames. *Combust. Flame*, 114:119–148, 1998.

[5] P. A. M. Kalt, Y. M. Al-Abdeli, A. R. Masri, and R. S. Barlow. Swirling turbulent non-premixed flames of methane: flow field and compositional structure. *Proc. Combust. Inst.*, 29:1913–1919, 2002.

[6] Y. M. Al-Abdeli and A. R. Masri. Stability characteristics and flowfields of turbulent non-premixed swirling flames. *Combust. Theory Modelling*, 7:731–766, 2003.

[7] Y. M. Al-Abdeli and A. R. Masri. Recirculation and flowfield regimes of unconfined non-reacting swirling flows. *Exp. Thermal and Fluid Science*, 27:655–665, 2003.

[8] A. R. Masri, S. B. Pope, and B. B. Dally. Probability density function computations of a strongly swirling nonpremixed flame stabilized on a new burner. *Proc. Combust. Inst.*, 28:123–131, 2000.

[9] F. K. Owen, L. J. Spadaccini, and C. T. Bowman. Pollutant formation and energy release in confined turbulent diffusion flames. *Proc. Combust. Inst.*, 16:105–117, 1976.

[10] C. D. Pierce and P. Moin. Progress variable approach for large-eddy simulation of non-premixed turbulent combustion. *J. Fluid Mech.*, 504:73–97, 2004.

[11] B. Janus, A. Dreizler, and J. Janicka. Flow field and structure of swirl stabilized non-premixed natural gas flames at elevated pressure. *ASME Turbo Expo*, GT2004-53340, Vienna, Austria, 2004.

[12] B. Janus, A. Dreizler, and J. Janicka. Experimental study on stabilization of lifted swirl flames in a model GT combustor. *Flow, Turb. Combust.*, 75:293–315, 2005.

[13] J. Smagorinsky. General circulation experiments with the primitive equations: I. the basic equations. *Mon. Weather Rev.*, 91:99–164, 1963.

[14] M. Germano, U. Piomelli, P. Moin, and W. H. Cabot. A dynamic subgrid-scale eddy viscosity model. *Phys. Fluids A*, 3(7):1760–1765, 1991.

[15] D. K. Lilly. A proposed modification of the germano subgrid-scale closure method. *Phys. Fluids A*, 4:633–635, 1992.

[16] M. Lésieur and O. Métais. New trends in large eddy simulation of turbulence. *Annu. Rev. Fluid Mech.*, 28:45–82, 1996.

[17] N. Peters. Laminar flamelet concepts in turbulent combustion. *Proc. Combust. Inst.*, 21:1231–1250, 1986.

[18] S. S. Girimaji and Y. Zhou. Analysis and modeling of subgrid scalar mixing using numerical data. *Phys. Fluids*, 8:1224–1236, 1996.

[19] J. A. van Oijen and L. P. H. de Goey. Laminar flamelet concepts in turbulent combustion. *Combust. Theory Modelling*, 6:463–478, 2002.

[20] A. W. Vreman, B. A. Albrecht, J. A. van Oijen, L. P. H. de Goey, and R. J. M. Bastiaans. Premixed and nonpremixed generated manifolds in large-eddy simulation of Sandia flame D and F. *Combust. Flame*, 153:394–416, 2008.

[21] N. Branley and W. P. Jones. Large eddy simulation of a turbulent non-premixed flame. *Combust. Flame*, 127:1914–1934, 2001.

[22] T. Landenfeld, A. Sadiki, and J. Janicka. A turbulence-chemistry interaction model based on a multivariate presumed beta-PDF method for turbulent flames. *Flow, Turb. Combust.*, 68:111–135, 2002.

[23] T. Lehnhäuser and M. Schäfer. Improved linear interpolation practice for finite-volume schemes on complex grids. *Int. J. Numer. Meth. Fluids*, 38(7):625–645, 2002.

[24] N. P. Waterson and H. Deconinck. Development of bounded higher-order convection scheme for general industrial applications. Project Report 1994-33, Von Karman Institute, 1994.

[25] CHEM1D. `http://www.combustion.tue.nl/chem1d/`.

[26] A. Ketelheun. Application and investigation of the flamelet generated manifolds theory with regard to mixture fractions beyond flammability limits. Master's thesis, TU Darmstadt, 2008.

[27] G. P. Smith, D. M. Golden, M. Frenklach, N. W. Moriarty, B. Eiteneer, M. Goldenberg, C. T. Bowman, R. K. Hanson, S. Song, W. C. Gardiner, Jr., V. V. Lissianski, and Z. Qin. GRI-Mech. `http://www.me.berkeley.edu/gri-mech/`.

[28] M. Klein, A. Sadiki, and J. Janicka. A digital filter based generation of inflow data for spatially developing direct numerical or large eddy simulation. *J. Comput. Physics*, 186:652–665, 2003.

[29] A. Kempf, R. P. Lindstedt, and J. Janicka. Large-eddy simulation of a bluff-body stabilized nonpremixed flame. *Combust. Flame*, 144:170–189, 2006.

[30] V. Raman, H. Pitsch, and R. O. Fox. Eulerian transported probability density subfilter model for large-eddy simulation of turbulent combustion. *Combust. Theory Modelling*, 10:439–458, 2006.

[31] V. Raman, H. Pitsch, and R. O. Fox. Hybrid large-eddy simulation/Lagrangian filtered-density-function approach for simulating turbulent combustion. *Combust. Flame*, 143:56–78, 2005.

[32] S. Navarro-Martinez and A. Kronenburg. LES-CMC simulations of a turbulent bluff body flame. *Proc. Combust. Inst.*, 31:1721–1728, 2007.

[33] C. Olbricht, F. Hahn, A. Ketelheun, and J. Janicka. PDF modeling strategies for LES of a bluff-body stabilized swirl combustor using premixed generated manifolds. In *Sixth International Symposium on Turbulence and Shear Flow Phenomena*, Seoul, South Korea, 2009.

[34] C. Olbricht, F. Hahn, and J. Janicka. Detailed numerical investigation of sydney bluff-body flames. *ERCOFTAC Symposium on Engineering Turbulence Modelling and Measurements*, 7:713–718, 2008.